Bubble Columns

N.G. Deen, Faculty of Science and Technology, Institute of Mechanics Processes and Control Twente (IMPACT), University of Twente, The Netherlands

R.F. Mudde, Multi-Scale Physics, Faculty of Applied Sciences, Delft University of Technology, The Netherlands

J.A.M. Kuipers, Faculty of Science and Technology, Institute of Mechanics Processes and Control Twente (IMPACT), University of Twente, The Netherlands

Peter Zehner, BASF Aktiengesellschaft, Ludwigshafen, Germany

Matthias Kraume, BASF Aktiengesellschaft, Ludwigshafen, Germany

Notation

Roman symbols

a: specific interfacial area, m^{-1}
A: interfacial area, m^2
Bo: Bodenstein number, dimensionless
c: concentration, mol/L
C_D: drag coefficient, dimensionless
C_L: lift cooefficent, dimensionless
d: diameter, m
D: diffusion or dispersion coefficient, m^2/s
$D_{G,\,L}$: diffusion coefficient of dissolved gas in liquid, m^2/s
e_M: energy dissipation rate per unit mass, W/kg
e_V: energy dissipation rate per unit volume, W/m^3
E_{in}: energy put into the system
Eo: Eötvös number, dimensionless
Fr: Froude number, dimensionless
g: gravitational acceleration, 9.81 m/s^2
Ga: Galileo number, dimensionless
h: height, m
h_R: height of gas–liquid mixture, m
h_t: height of reactor, m
j: superficial velocities, m/s
J_D: dispersion flow, m/s
k_L: liquid-phase mass-transfer coefficient, m/s
K: total friction factor
l_m: mixing length, m
n: bubble number density, dimensionless
M: relative size of the separator, dimensionless
P: power, W
Δp: pressue drop, Pa
Pr: Prandtl number, dimensionless
R: radius of the riser, m
Re: Reynolds number, dimensionless
Sh: Sherwood number, dimensionless
St: Stanton number, dimensionless
t: time, s
u: superficial velocity, m/s
$\bar{u}_g$: local gas velocity, m/s

10.1002/14356007.b04_275.pub2

u_G^*: bubble swarm velocity, m/s
v: velocity, m/s
v_{rG}: relative velocity of bubble swarm in liquid, m/s
$\tilde{v}_s$: slip velocity, m/s
V: volume, m^3
We: Weber number, dimensionless
z: axial coordinate, m

Greek symbols

α: heat transfer coefficient, W K^{-1} m^{-2}
ε: volume fraction
ε_G: gas holdup, dimensionless
ε_R: radial gas fraction
μ: viscosity, Pa·s
ρ: density, kg/m^3
τ: stress tensor, N/m^2
σ: surface tension, N/m
Φ_G: gas inflow rate, m^3/s

Subscripts

b: bubble
bS: Sauter diameter
D: downflow
G: gas phase
h: hole
H: horizontal bubble diameter
i: inside draft tube
L: liquid
max: maximum value
min: minimum value
M: per unit mass
n: nozzle
r: relative
R: upflow, reaction mixture
s: slip
t: reactor

1. Introduction

Bubble columns are devices in which gas, in the form of bubbles, are brought into contact with liquid. In their simplest form, bubble columns may be used to purely mix the liquid phase. However, more often, bubble columns are used to transfer chemical species from one phase into the other, for example, when gaseous reactants are dissolved in a liquid or when liquid reaction products are stripped. Both processes can take place simultaneously. A chemical or biological reaction nearly always proceeds in the liquid phase. Depending on the application, special measures to intensify mass transfer between the two phases may be useful, or the residence-time distribution of one or both phases may be modified.

The liquid may also contain inert, catalytically active, or reactive particles in suspension. Oxidation, hydrogenation, chlorination, phosgenation, alkylation, and other processes have long been performed in bubble column reactors in the chemical industry. Industrial reactors for high-tonnage products have capacities of 100–300 m^3. Larger bubble columns, with capacities up to 3000 m^3, are employed as fermenters for protein production from methanol. The largest units (20 000 m^3) are those for waste water treatment.

Since the 1970s bubble columns have gained considerable scientific interest. This led to the development of many empirical correlations and theoretical models enabling the mathematical simulation of bubble column reactors. Since the late 1990s increasing efforts have been made to model bubble columns with the aid of computational fluid dynamics (CFD, → Computational Fluid Dynamics). This has led to an improved understanding in the detailed flow phenomena and related (chemical) conversions in these apparatus. However, the detailed predictions of coalescence and breakup of bubbles is still difficult as well as the correct prediction of bubble columns operating in the industrially important heterogeneous regime.

The mixing of a liquid and a gas having only partial mutual solubility is one of the unit operations in chemical engineering. As Figure 1 shows, this operation takes one of two main forms. The simplest design is the bubble column (Fig. 1A) in which gas is fed into the column at the bottom and rises in the liquid, escaping from it at the free surface; the gas is consumed to a greater or lesser extent (depending on the intensity of mass transfer and chemical reaction). When the off-gas contains high concentrations of valuable reactants, part of it is recycled to the reactor. This recycle design, however, lowers the concentration profile in the bubble column

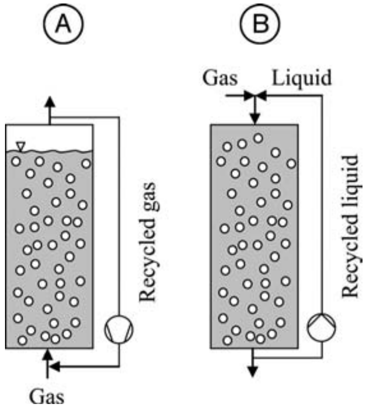

Figure 1. Principal methods of gas–liquid mixing
A) Bubble column; B) Downflow bubble column

and must be optimized from an economic standpoint. In a simple bubble column the liquid flows either co-currently or counter-currently to the upward gas stream and has a long residence time. The flow direction of the liquid phase has little effect on the gas-phase residence time, which is much shorter than the liquid-phase residence time. Thus, in the simple column, the flow of gas is always from bottom to top, and the stream can be composed of both fresh and recycle gas.

Longer gas-phase residence times can be achieved with the downflow bubble column shown in Figure 1B. The liquid is pumped down through the column at a velocity of more than 20 cm/s, so that gas let in at the top is entrained by the downflowing liquid and can even be held in a suspension-like state until it has reacted completely. Usually, however, unconsumed gas is removed with the liquid and separated. Special designs permit phase separation inside the apparatus. The downflow bubble column is used mainly when large liquid streams are to be contacted with small gas streams, and a short liquid residence time is required. The necessary velocity cannot always be obtained with the liquid inlet to the reactor. Thus, like the gas in an ordinary bubble column, the liquid in the downflow bubble column can be recycled. Typical applications for downflow bubble columns are the ozonation of drinking water and the treatment of water in swimming pools.

In both types of column energy must be supplied continuously to the two-phase system to keep the liquid and gas mixed. Only in this way can separation of the phases be counteracted or reversed. In the simple bubble column, this energy is supplied by the gas and in the downflow bubble column by the downflowing liquid.

These two basic methods of dispersing gas in liquid are generally not used in their pure forms. The variety of problems in chemical and biotechnical processes has led to many different contacting devices that combine these basic techniques.

2. Bubble Columns

2.1. Design and Applications

Bubble columns are very adaptable gas–liquid contacting devices; possible designs are shown in Figure 2. The simplest form of bubble column

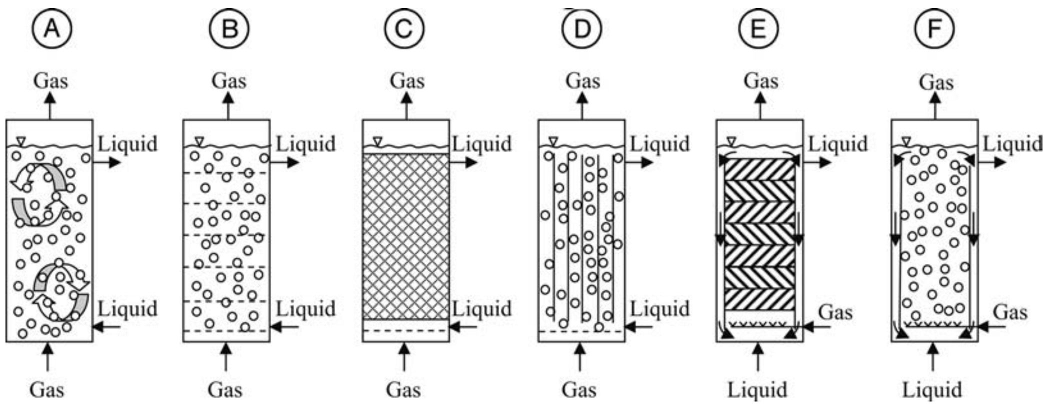

Figure 2. Types of bubble column reactors
A) Simple bubble column; B) Cascade bubble column with sieve trays; C) Packed bubble column; D) Multishaft bubble column; E) Bubble column with static mixers; F) Airlift loop reactor

(Fig. 2A) consists of a vertical tube with no internals. Gas is fed in at the bottom while liquid is led through the apparatus co-currently or counter-currently. This simple form is seldom used in practice; instead, a number of modifications are employed. The backmixing of gas and liquid phases in the simple bubble column and the nonuniform distribution of gas bubbles over the cross section can be reduced by the installation of trays (Fig. 2B), packings (Fig. 2C), or shafts (Fig. 2D). All these devices can operate either co-currently or counter-currently. To set up the most homogeneous possible bubble flow, static mixer elements can also be placed in the ascending flow section (Fig. 2E). One can use the action of gravity to generate a global circulation as it is done in airlift loop reactors (Fig. 2F) which is described in detail in Section 3.

2.2. Gas Distribution

Usually, the gas is dispersed to create small bubbles and distribute them uniformly over the cross section of the equipment to maximize the intensity of mass transfer. The formation of fine bubbles is especially desirable in coalescence hindered systems and in the homogeneous flow regime (Section 2.3). In principle, however, significant mass transfer can be obtained at the gas distributor through a high local energy dissipation density [1, 2].

In most cases, gas bubbles are generated by pores or holes or in the shear zone of a liquid jet. Figure 3 shows typical forms of "*static*" *gas spargers*, in which bubble formation occurs without any external energy supply. The simplest of these devices, the dip tube (Fig. 3A), gives only an acceptable uniform gas distribution over the cross section at some distance above the sparger. Perforated plates (Fig. 3B) and perforated ring spargers (Fig. 3C) are more effective. Both require a minimum gas flow rate to achieve uniform distribution and prevent the liquid from getting into the sparger [3–5]. Very fine bubbles can be generated using porous plates (Fig. 3D), but their pores are susceptible to fouling, and this type of sparger is seldom used in full-scale equipment.

An alternative offer *dynamic spargers* which use the power of a liquid jet to disperse gas in a zone of high energy dissipation rate [6–8]. Figure 4 illustrates several frequently used dynamic gas spargers. The simple two-phase jet nozzle alone (Fig. 4A) or with momentum-transfer tube (Fig. 4B) is not able to simultaneously disperse gas and suck in the gas stream. This can be achieved, however, with the ejector jet nozzle (Fig. 4C), the ejector (Fig. 4D), and the Venturi tube (Fig. 4E). During nozzle selection the ratio of the gas–liquid volumetric flow rates must always be considered. Common values lie between 0.5 and 2. However, much higher values can be achieved in special cases with momentum-transfer tubes [7].

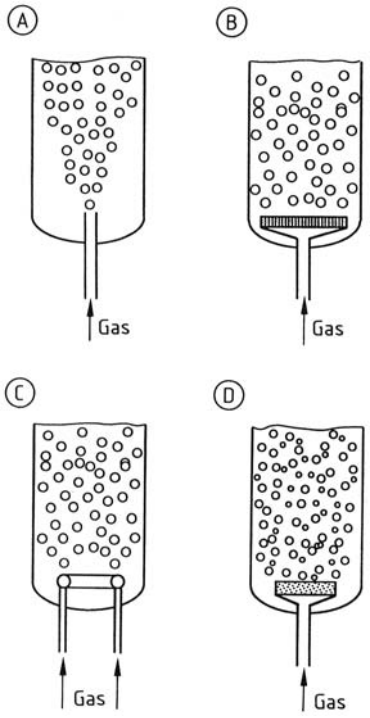

Figure 3. Static gas spargers
A) Dip tube; B) Perforated plate; C) Perforated ring sparger; D) Porous plate

2.3. Flow Regimes

The flow in bubble columns can be divided into three main regimes. These regimes are characterized by the superficial gas velocity and the reactor diameter. In the *homogeneous flow regime* the gas–liquid mixture is composed of

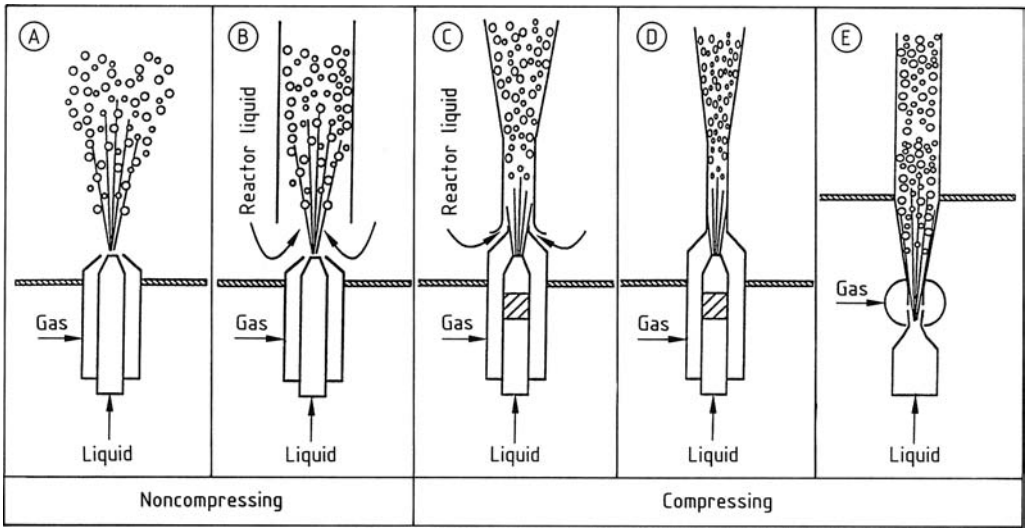

Figure 4. Dynamic gas spargers
A) Two-phase jet nozzle; B) Two-phase jet nozzle with momentum-transfer tube; C) Ejector jet nozzle; D) Ejector; E) Venturi nozzle

bubbles with a narrow bubble-size distribution that are dispersed relatively uniformly over the cross section of the apparatus. This regime extends to superficial gas velocities of 0.03–0.08 m/s, depending on the gas–liquid system and gas sparger type.

The uniform distribution of gas bubbles vanishes at higher gas rates, due to prevalence of coalescence, and a highly turbulent flow structure develops. In this *heterogeneous* or *churn-turbulent flow regime*, large bubbles form and travel upward at high velocity (see Section 2.6), mainly near the column axis. The circulating flow that results may be so vigorous that bubbles of a size corresponding to that in the homogeneous regime are actually transported downward in the zone near the column wall (see Fig. 5 and Section 2.4).

In columns of a small diameter, often used in the laboratory, *slug flow* occurs at high gas flow rates. Large bubbles encompassed by the column wall take a characteristic elongated slug shape.

The relationship between superficial gas velocity and reactor diameter is illustrated by the flow map of Figure 6 [10]. The broad transition regions are due to the effects of the gas distributor, the gas–liquid system, and the liquid rate. Knowledge of the flow regime is particularly important because it strongly affects the productivity of bubble column reactors. An extensive review of these dependencies can be found in the work of Shaikh and Al-Dahhan [11].

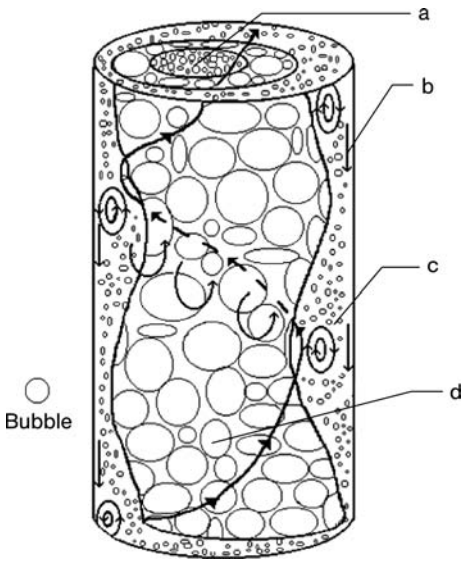

Figure 5. 3D flow structure in bubble columns proposed by Chen et al. [9] in the heterogeneous flow regime
a) Central plum region; b) Descending flow region; c) Vortical-spiral flow region; d) Fast bubble flow region

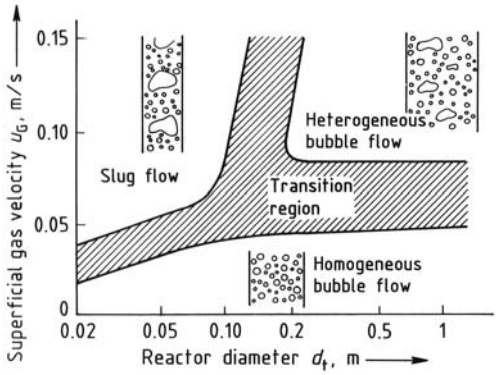

Figure 6. Flow regimes in a bubble column after SHAH et al. [10]

2.4. Bubble Size

Analysis of bubble size in bubble columns must distinguish between bubble-size distribution just after bubble formation at the sparger and size distribution further away from the distributor. Because of breakup and coalescence of the rising bubbles, the two distributions can differ significantly. An extensive review of bubble formation at orifices was made by KULKARNI and JOSHI [12]. The process of bubble formation is governed by many operating parameters (i.e., gas flow rate through the orifice, mode of operation, flow/static condition of the liquid), system properties (i.e., orifice dimensions, orifice chamber volume), and also the physicochemical properties, such as liquid viscosity, liquid density, and polarity of the liquid, etc., which decide the mode of bubble formation and subsequently reflects on bubble size.

The size at which bubbles are formed at the sparger is usually quickly altered due to coalescence and/or breakup. Since the efficiency of bubble columns depends primarily on bubbles far from the gas distributor, the following discussion only concerns these.

There are two basic methods — photography and probe techniques — for determining bubble size; however, they do not lead to identical results. Both methods are subject to certain limitations in view of the marked bubble selection that may occur (i.e., not all bubble sizes can be detected) [13, 14]. In particular, any measurement method only leads to realistic results if the flow is homogeneous (i.e., a narrow bubble-size distribution is found). So far, no method can be recommended for the measurement of large bubbles in the heterogeneous flow regime.

For bubbles that are present in a region of high turbulence, the following formula can be used to describe the Sauter diameter d_{bS} (mean bubble diameter, calculated from the volume to surface ratio) [15–17]. Using Kolmogorov's theory of isotropic turbulence, the bubble diameter can be expressed in terms of the Weber number, We, which balances the inertia and surface forces acting on the bubble

$$We = \frac{\tau}{\sigma/d_b} \quad \text{with} \quad \tau = \rho_L \overline{v^2} = 2\rho_L (e_M d_b)^{2/3}$$

$$d_{bS} = \left(\frac{We}{2}\right)^{0.6} \left(\frac{\sigma}{\rho_L}\right)^{0.6} \left(\frac{1}{e_M}\right)^{0.4}$$

where σ is the surface tension and e_M the turbulent kinetic energy dissipation.

Another relationship often used, was proposed by AKITA and YOSHIDA who used photographic methods to determine bubble size distributions for various systems:

$$\frac{d_{bS}}{d_t} = 26 \left(\frac{d_t^2 g \rho_L}{\sigma}\right)^{-0.5} \left(\frac{d_t^3 g}{\nu_L^2}\right)^{-0.12} \left(\frac{u_G}{\sqrt{g d_t}}\right)^{-0.12}$$

When static gas spargers are used, the bubble diameter is only weakly dependent on the gas velocity. Descriptive correlations [18–21] are applicable only to systems and sparger geometries for which they were obtained; a generally valid description of bubble size is not available yet. The maximum bubble diameter $d_{b,max}$ can be used for estimation purposes [14, 22].

In case of relatively mild flow conditions, the inertial force will be small compared to the surface force action on the bubble. In that case, the maximum bubble size is determined by internal centrifugal force and the surface force, yielding the following expression [23]:

$$d_{b,max} = 2.53 \sqrt{\frac{\sigma}{g \rho_G}}$$

For the water–air system at ambient conditions this relation yields $d_{b,max} = 20$ cm, however, in experiments a maximum bubble size of about 10 cm was found. Larger bubbles have a high probability of being unstable and thus break up. The Sauter diameter for real distributions is between 40 and 60% of the largest stable

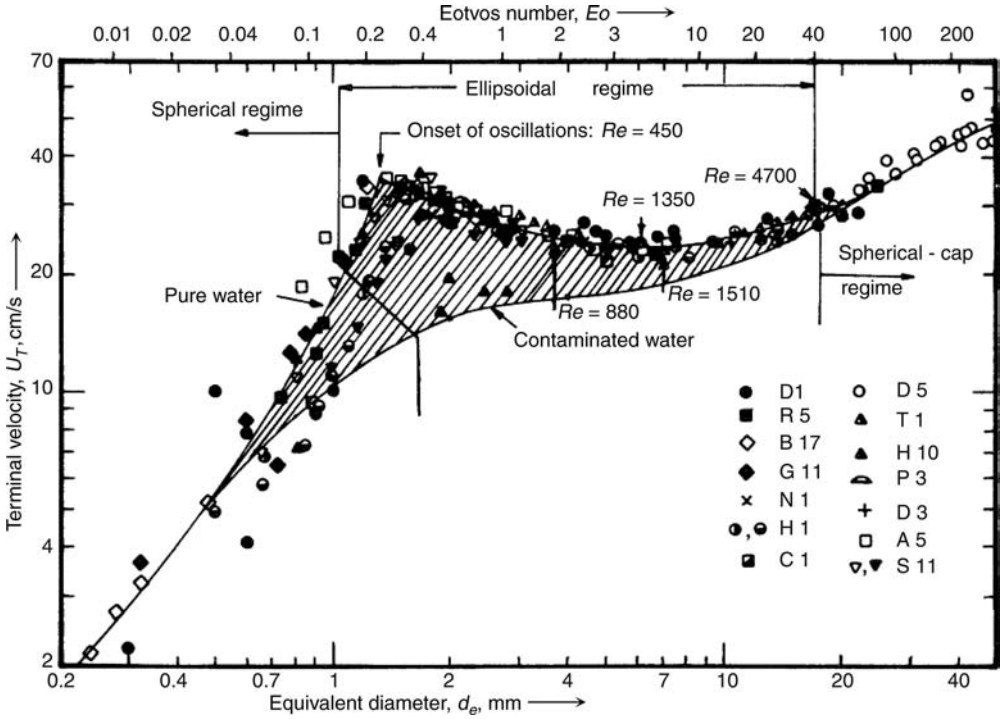

Figure 7. Terminal velocity of air bubbles in water at 20°C [24]

bubble diameter. This estimate is not applicable to the heterogeneous flow regime due to the bimodal bubble-size distribution in this regime. Note that the dependency on the gas density can be used to decrease the maximum bubble size and to improve the operation by increasing the operation pressure.

2.5. Bubble Rise Velocity

In the homogeneous flow regime, bubbles keep the same size as they were released from the sparger, since coalescence and breakup hardly take place. As a result, bubbles of almost uniform size and shape rise in the form of a swarm distributed uniformly over the column cross section. The bubble slip velocity (i.e., the difference between the bubble velocity and the local liquid velocity) is correlated to the bubble size and depends strongly on the presence of surface active agents, as shown in Figure 7 [24].

In the heterogeneous flow regime, small and large bubbles coexist [25, 26]. The large bubbles are formed because of coalescence and rise at a substantially higher velocity than the small bubbles. Figure 8 shows velocities for large and small bubbles [25]. Large bubbles first appear at a superficial gas velocity of about 0.03 m/s. The formation of large bubbles, however, depends strongly on the type of sparger used. With sintered plates, for example, larger bubbles first

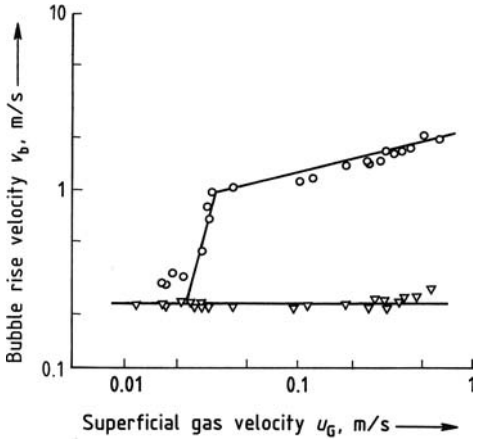

Figure 8. Velocities of rising bubbles for the system water–air reactor: $d_t = 0.44$ m, $h_t = 5$ m; Gas distributor: perforated plate ($d_h = 3$ mm) [25] (○) Large bubbles; (▽) Small bubbles

start to appear at gas rates higher than 0.1 m/s. Large bubbles have a rise velocity that is four or more times larger than that of small bubbles (Fig. 8). Thus, most of the gas transport in the heterogeneous flow regime is accomplished by large bubbles. In this regime, the quantity of gas transported by small bubbles remains more or less constant, whereas the quantity transported by large bubbles increases linearly with gas velocity. This relationship applies to coalescing and coalescence-hindered gas–liquid systems.

2.6. Axial Dispersion

Because of the large-scale circulation flows, backmixing occurs in both phases. Axial dispersion models characterize the backmixing by only a single parameter. Its simplicity makes that it is widely used to describe the non-ideal mixing behavior in bubble column reactors. The dispersion flow, J_D, can be expressed in analogy with Fick's diffusion law:

$$J_D = -D_L \frac{dc}{dz}$$

The dispersion coefficient D_L is essentially a function of the superficial gas velocity and the column diameter. Flow direction or liquid velocity do not show any effect, provided the superficial liquid velocity remains within the range common in industry ($u_L < 0.03$ m/s). The dispersion coefficient can be estimated fairly accurately on the basis of fluid dynamic models. Riquarts [27] suggest the use of the following model for the dispersion coefficient:

$$D_L = 0.065 g^{1/2} d_t^{3/2} \left(\frac{u_G^3}{g \nu_L} \right)^{1/8}$$

Clearly, the dispersion coefficient is strongly dependent on the column diameter.

Another relation often used, was proposed by Baird and Rice [28], which is based on Kolmogorov's theory of isotropic turbulence:

$$D_L = 0.35 g^{1/3} u_G^{1/3} d_t^{4/3}$$

The axial dispersion of the gas phase depends on the formation of large and small bubbles, coalescence and breakup. In bubble columns with a small diameter, the gas phase shows virtually no backmixing. Contrary, large units behave more like stirred tanks, showing considerable backmixing.

Van Baten and Krishna [29] showed that the gas phase axial dispersion coefficient for small bubbles is very close to that of the liquid phase, suggesting that small bubbles are entrained with the liquid phase and have similar backmixing characteristics. The dispersion of large bubbles is very small, indicating that large bubbles rise relatively undisturbed through the reactor and can be described by a plug flow model.

A good expression for the axial dispersion of the gas phase was proposed by Mangartz and Pilhofer [30]:

$$D_G = 5 \times 10^{-4} u_G^{*3} d_t^{3/2}$$

When this relation is used to compute the Bodenstein number, *Bo*, (ratio between axial convective transport and axial dispersion) for typical systems, one finds:

$$Bo = \frac{u_G h_R}{D_G \varepsilon_G} = 2 \times 10^3 \frac{\varepsilon_G^2 h_R}{u_G^2 d_t^{3/2}} = 2 \times 10^3 \frac{O(0.2)^2 O(600)}{O(5)^2 O(30)^{3/2}} = O(12)$$

which corresponds in practice to plug flow behavior of the gas phase, confirming the conclusion of Van Baten and Krishna [29].

2.7. Gas Holdup

Gas holdup is one of the most important operating parameters because it not only governs phase fraction and gas-phase residence time but is also crucial for mass transfer between liquid and gas. Gas holdup depends chiefly on the gas flow rate, but also to a great extent on the gas–liquid system involved. Accordingly, many correlations that have been published only apply to the systems investigated.

Gas holdup, ε_G, is defined as the volume of the gas phase divided by the total volume of the dispersion:

$$\varepsilon_G = \frac{V_G}{V_G + V_L} = \frac{h_R - h_0}{h_R}$$

where h_R and h_0 indicate the height of the free surface in the bubble column with and without gas sparging, respectively. The relationship between gas holdup and gas velocity is generally described by the proportionality:

$$\varepsilon_G \sim u_G^n$$

In the homogeneous flow regime, n is close to unity. When large bubbles are present, the

exponent decreases, i.e., the gas holdup increases less than proportionally to the gas flow rate. The higher the contribution of large bubbles to the total gas holdup, the smaller is the exponent n. In the fully developed heterogeneous flow regime, n has values between 0.4 and 0.7, depending on the gas–liquid system.

The effect of physical properties on gas holdup is very complex. Increasing the viscosity of the liquid phase leads to increased bubble coalescence and thus a decrease in gas holdup. Above ca. 50 m Pa s the gas holdup remains constant [31]. Although surface tension is not very important for the gas holdup, a change in coalescence behavior may have lasting effects. The relation of AKITA and YOSHIDA [32] is suitable for estimating the gas holdup and is based on the investigation of numerous systems:

$$\frac{\varepsilon_G}{(1-\varepsilon_G)^4} c_1 = \left(\frac{g d_t^2 \rho_L}{\sigma}\right)^{\frac{1}{8}} \left(\frac{g d_t^3}{\nu_L}\right)^{\frac{1}{12}} \left(\frac{u_G}{\sqrt{g d_t}}\right)$$

For pure liquids and nonpolar solutions the constant c_1 is 0.2, for electrolyte solutions it is 0.25. However, reliable results cannot be expected for systems that have not been investigated in this study.

The effects of reactor pressure on gas holdup have not been fully explained. Although some authors find no effect between 1 and 16 bar [33], others find that gas holdup increases with pressure in systems with small sparging holes (d_h 1 mm) or with sintered plates [34–37]. Transition from the homogeneous to the heterogeneous regime occurs at higher gas flow rates as pressure increases.

Gas holdup is generally a function of position in the bubble column. Axial profiles of gas holdup show a zone near the gas distributor in which the holdup increases to the value that characterizes the following equilibrium zone. The gas holdup at the top of the column, in the zone of bubble breakup, is markedly higher than the equilibrium value [38].

Gas holdup also depends on radial position. The profile shows gradients only near the wall in the homogeneous flow regime [38–40]. In contrast, a parabolic radial gas holdup distribution appears in the heterogeneous regime [26, 38, 39], as a consequence of the preferential rising of large bubbles or agglomerates of bubbles in the axis of the column.

2.8. Specific Interfacial Area

The area of the gas–liquid interface is one of the most important process parameters. Especially at high reaction rates (e.g., when a bubble column is employed as an absorber), the interfacial area becomes a crucial factor in equipment sizing. Like gas holdup, interfacial area depends on the geometry, operating conditions, and gas–liquid system. Gas holdup and interfacial area per unit volume are related as

$$a = \frac{A}{V_R} = \frac{6\varepsilon_G}{d_{bS}}$$

where V_R is the volume of the reaction mixture and d_{bS} is the Sauter diameter (Section 2.5). When applying the formula to the relationship of AKITA and YOSHIDA the following expression is obtained:

$$a d_t = 0.23 \left(\frac{d_t^2 g \rho_L}{\sigma}\right)^{1/2} \left(\frac{d_t^3 g}{\nu_L^2}\right)^{0.12} \left(\frac{u_G}{\sqrt{g d_t}}\right)^{0.12} \varepsilon_G$$

which for small columns ($d_t < 0.14$ m) can be simplified to:

$$a d_t = \frac{1}{3} \left(\frac{d_t^2 g \rho_L}{\sigma}\right)^{1/2} \left(\frac{d_t^3 g}{\nu_L^2}\right)^{0.1} \varepsilon_G^{1.13}$$

2.9. Mass Transfer

The mass transfer between the gas and liquid phase in a bubble column can be generally described by the volumetric mass-transfer coefficient $k_L a$, which is the liquid-phase mass-transfer coefficient k_L multiplied by the specific interfacial area. Gas-phase resistance can usually be neglected, so $k_L a$ gives an adequate description. To determine the mass-transfer rate, however, the driving concentration difference must be known which in turn requires knowledge of mixing behavior in the gas and liquid phase. In industrial units ($d_t > 1$ m), estimates can be based on the assumption of complete mixing in both liquid and gas phases.

Like gas holdup and interfacial area, $k_L a$ also depends on the gas flow rate, type of sparger, and gas–liquid system. The mass-transfer coefficient and the gas rate are proportional to one another:

$$k_L a \sim u_G^n$$

where n can be between 0.7 and 0.92 [18, 41–44].

Mass-transfer coefficients of two- to threefold higher can be achieved in the homogeneous flow regime if a porous plate is used as a sparger instead of a perforated plate. In the heterogeneous regime the effect of the sparger is negligible.

According to experimental results, the column diameter above 15 cm has no effect on mass-transfer coefficient. Some correlations include nonetheless reactor diameter [18, 42, 45]. AKITA and JOSHIDA [18] state that the value of the column diameter used for calculation should not be increased beyond 0.6 m. Based on this premise, their correlation for k_La is

$$\frac{k_L a d_t^2}{D_{G,L}} = 0.6\left(\frac{\nu_L}{D_{G,L}}\right)^{1/2}\left(\frac{g d_t^2 \rho_L}{\sigma}\right)^{0.62}\left(\frac{g d_t^3}{\nu_L^2}\right)^{0.31}\varepsilon_G^{1.1}$$

and has the best experimental support.

The mass-transfer coefficient increases in coalescence hindered systems [46, 47]. This increase depends on the system and the concentration of coalescence-hindering substance. The maximum gain in mass-transfer coefficient due to the presence of electrolytes, however, is only 30%.

2.10. Heat Transfer

In many cases, heat must be removed when operating bubble columns. A particularly simple solution is to use the latent heat of vaporization of the liquid phase for heat removal, although this is not always feasible. In addition, there are many possibilities for heat transfer through heated or cooled surfaces. Thus, up to ca. 30 m^2/m^3 of heat-transfer area can be installed in a bubble column.

The turbulent flow generated by rising gas bubbles increases heat transfer even at low gas rates. The increase in heat-transfer coefficient α, with gas throughput is markedly greater in the homogeneous than in the heterogeneous regime.

The heat-transfer coefficient is independent of the column diameter, type of sparger, or coalescence behavior of the gas–liquid system.

A good relation for the liquid to wall heat-transfer coefficient is given by DECKWER et al. [46] who performed heat transfer measurements for a single tube immersed in a bubble column.

$$St = 0.1(ReFrPr^2)^{-1/4}$$

$St = \frac{\alpha}{\rho C_p u_G}$, $Re = \frac{u_G d_{bS} \rho_L}{\mu_L}$, $Fr = \frac{u_G^2}{g d_{bS}}$, and $Pr = \frac{\mu C_p}{k}$ are the dimensionless Stanton, Reynolds, Froude, and Prandtl numbers, respectively.

For tube bundles arranged in an axial direction, the heat-transfer coefficient increases with increasing tube pitch and decreases when the free cross-sectional area increases. A similar relationship is found for a tube bundle arranged in cross flow, but here a marked effect of liquid throughput occurs.

The installation of tube bundles leads to an overall change in fluid dynamics and thus in mixing behavior. For example, tubes installed in cross flow hinder flow in the longitudinal direction and consequently reduce dispersion in the liquid phase. In contrast, the arrangement of heat-transfer surfaces in the flow direction leads to more intense mixing of the liquid phase by intensifying circulation.

An extensive review of heat transfer in two-phase and three-phase (slurry) bubble columns can be found in the work of HULET et al. [48].

2.11. Fluid Dynamics

To describe the hydrodynamics in bubble columns there are various types of models available, the choice of which depends on the level of detail that is required. The most commonly used model types are illustrated schematically in Figure 9.

Phenomenological models (Fig. 9A) are those models which describe the flow phenomena in an approximate manner, by assuming either plug flow behavior (PFR = plug flow reactor), ideal mixing (CISTR = continuous ideally stirred tank reactor) or axial dispersion (ADM = axial dispersion model). These models are relatively simple to construct and to solve and give first impressions of the performance of a bubble column reactor. These models rely on macroscopic properties that have to be determined experimentally or which are obtained from empirical correlations. The latter involves parameters such as bubble size, axial dispersion, specific area, etc., that were described in the previous sections. For lab-scale columns

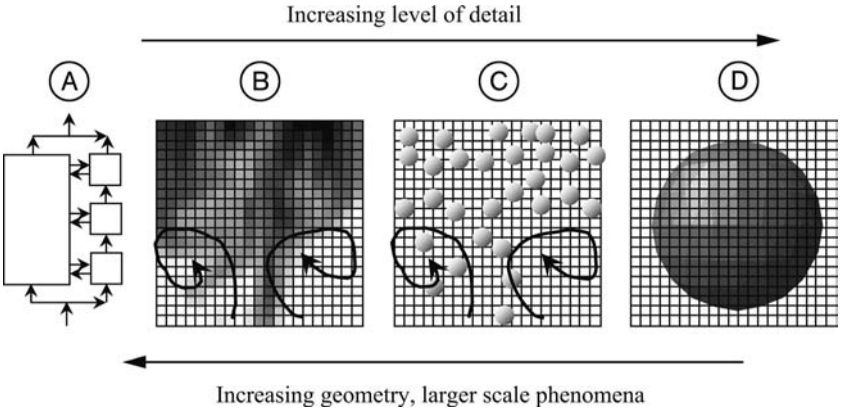

Figure 9. Schematic overview of gas–liquid hydrodynamic models
A) Phenomenological models; B) Two-fluid model; C) Discrete bubble model; D) Direct numerical simulations

usually plug flow behavior is assumed for the gas phase, whereas CISTR or ADM description is used for the liquid phase. For industrial columns that show significant backmixing of the gas phase, ADM models are typically used for both gas and liquid phases. A complete overview of which combination for each of the phases should be used, can be found elsewhere [46].

The described models rely on a 'single cell' assumption, i.e., the change of relevant properties can be described by a single differential equation. JOSHI and SHARMA [49] proposed a cell model that divides the bubble column into zones for which a partial differential equation is solved. In this model backflow can be considered. Furthermore, such model can account for a certain degree of locality, i.e., axially dependent gas velocity and/or pressure gradient.

Often, a more detailed description of the fluid dynamics in a bubble column is required [50, 51]. To this end computational fluid dynamics (CFD) models can be used. In essence these are similar to the cell model described above, with the major difference that no assumptions are made on the gas and liquid (back-) flow. Instead, the gas and liquid phase hydrodynamics are result of the model and depend on the geometrical description of the column (height, width, sparger configuration). In CFD models the liquid phase hydrodynamics is described by dividing the bubble column into computational cells of small size (typically 1 cm), for which mass, momentum, and energy balances are being solved. The description of the gas phase can be done in roughly three ways as indicated in Figure 9.

The Euler–Euler or two-fluid model (TFM, Fig. 9B) is mostly used for industrial applications. In this model, the properties of the gas phase are volume averaged to obtain a continuum description, similar to the liquid phase, while taking the interfacial forces due to interfacial drag, transverse lift and added mass into account. Since this model takes a continuum approach, it does not consider variations related to individual bubbles, which can be substantial in the heterogeneous flow regime as pointed out earlier. One can explain coalescence and breakup, assuming isotropic turbulence as described in Section 2.4. However, the description is complicated by the fact that locally only one characteristic bubble size is used, whereas in practice there might be a distribution in bubble size. Typical systems involve computational grids up to 10^6 cells, which corresponds to a bubble column with a volume of 1 m^3, assuming a computational grid size of 1 cm^3. A typical simulation result of a TFM simulation extended with a bubble number density equation is shown in Figure 10 [52] where a bubble number density equation is used:

$$\frac{\partial n}{\partial t} + \nabla \cdot (\bar{u_g} n) = 0$$

where n is the bubble number density and $\bar{u_g}$ is the local gas velocity. Note that n only can change due to advection, i.e., movement of

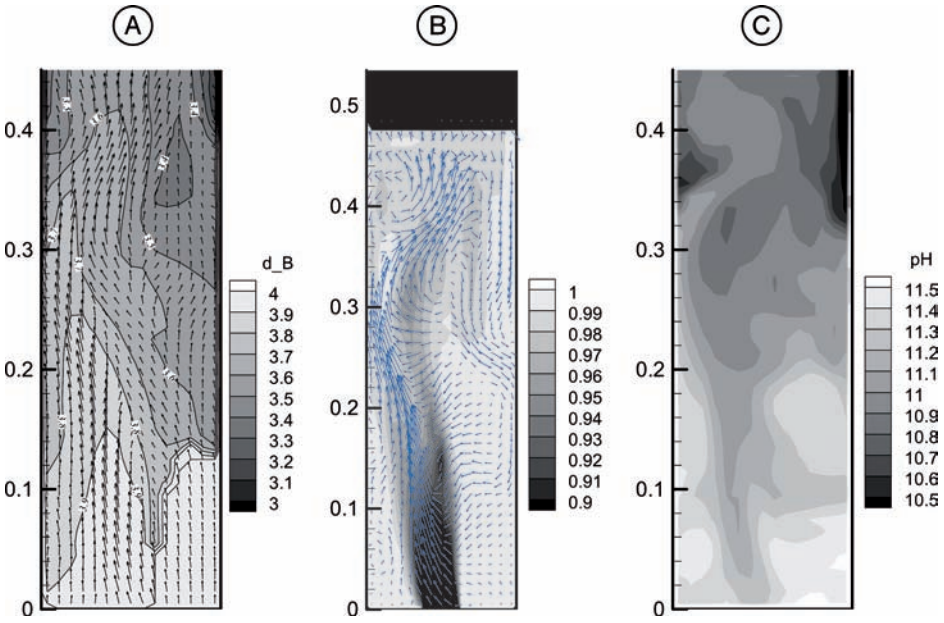

Figure 10. Instantaneous simulation result of a two-fluid model simulation of chemisorption of CO_2 in an aqueous sodium hydroxide solution with an initial pH = 12.0, 20 s after the CO_2 gas is introduced
A) Instantaneous bubble size distribution and gas phase velocity field; B) Liquid phase volume fraction and velocity field; C) pH distribution

bubbles. The local Sauter mean bubble diameter can easily be obtained using the gas phase continuity equation and bubble number density equation:

$$d_{bS} = \left(\frac{6\varepsilon_G}{\pi n}\right)^{1/3}$$

This example involves flow in the homogeneous flow regime, where breakup and coalescence can be neglected, so one can obtain information on the *global* bubble size distribution by using only one extra partial differential equation for the bubble number density. In heterogeneous flows, however, coalescence and breakup are of eminent importance and give rise to a *local* bubble size distribution. This can be described by solving a set of bubble number density equations, also known as population balance equations:

$$\frac{\partial n_i}{\partial t} + \nabla\cdot(\bar{u_{g,i}} n_i) = B_{B,i} - D_{B,i} + B_{C,i} - D_{C,i}$$

where n_i is the bubble number density of bubble size class i. The terms on the right hand side represent birth (B) and death (D) of bubbles within the size class due to breakup (subscript B) and coalescence (subscript C), respectively. Breakup is often modeled considering local Weber numbers following the theory described in Section 2.4. Coalescence is usually modeled as the product of bubble collision frequency and coalescence efficiency. Several breakup and coalescence closure models have been proposed, which are reviewed very well by Jakobsen et al. [51].

To truly describe the local bubble size distribution a set of about 25 population balance equations and associated momentum equations are required for each of the involved gas phases which makes the model computationally very expensive. This problem can partially be overcome by assuming a mutual gas velocity for each of the bubble size classes, which is reasonable for bubbles with diameters between 1 and 20 mm. This reduces the number of gas phase momentum equations to one and is known as the MUSIG model [53, 54]. Alternatively, the bubble size distribution can be characterized statistically, e.g., by calculating six moments of the bubble size distribution, rather than 25 bubble size classes in the population balance approach [55–57].

If one wants to describe exchange of mass, heat and momentum of individual bubbles, an Euler–Lagrange or discrete bubble model (DBM, Fig. 9C) can be used. In the DBM, each of the bubbles in the system is tracked by solving a force balance for each bubble, taking all relevant forces into account. The DBM has the advantage that, in contrast to the TFM, the bubble size distribution is part of the solution. The disadvantage of the DBM is that it is computationally more expensive than TFM, because all bubbles have to be tracked. Typical systems involve up to 10^6 bubbles, which corresponds to a bubble column with a volume of 1 m^3, assuming a bubble size of 6 mm and a holdup of 10%. A typical simulation result of a DBM simulation is shown in Figure 11 [58].

Both the TFM and the DBM rely on an accurate description of the interfacial forces between gas and liquid. For isolated bubbles a wealth of information is available for various gas–liquid combinations based on several experimental studies. For practical purposes the relation for the interfacial drag coefficient C_D proposed by Tomiyama [59] is recommended:

$$C_D = \max\left[\min\left(\frac{16}{Re}(1+0.15\,Re^{0.687}), \frac{24}{Re}\right), \frac{8}{3}\frac{Eo}{Eo+4}\right] \quad (1)$$

$$C_D = \max\left[\min\left(\frac{24}{Re}(1+0.15\,Re^{0.687}), \frac{72}{Re}\right), \frac{8}{3}\frac{Eo}{Eo+4}\right] \quad (2)$$

Equations 1 and 2 are used for pure systems and slightly contaminated systems, respectively.

For the added mass force, usually a force coefficient of 0.5 can be used. The direction of the lift force depends on the bubble size (small bubbles tend to move towards the wall, whereas large bubbles move to the centre of the column). The following relation for the lift coefficient,

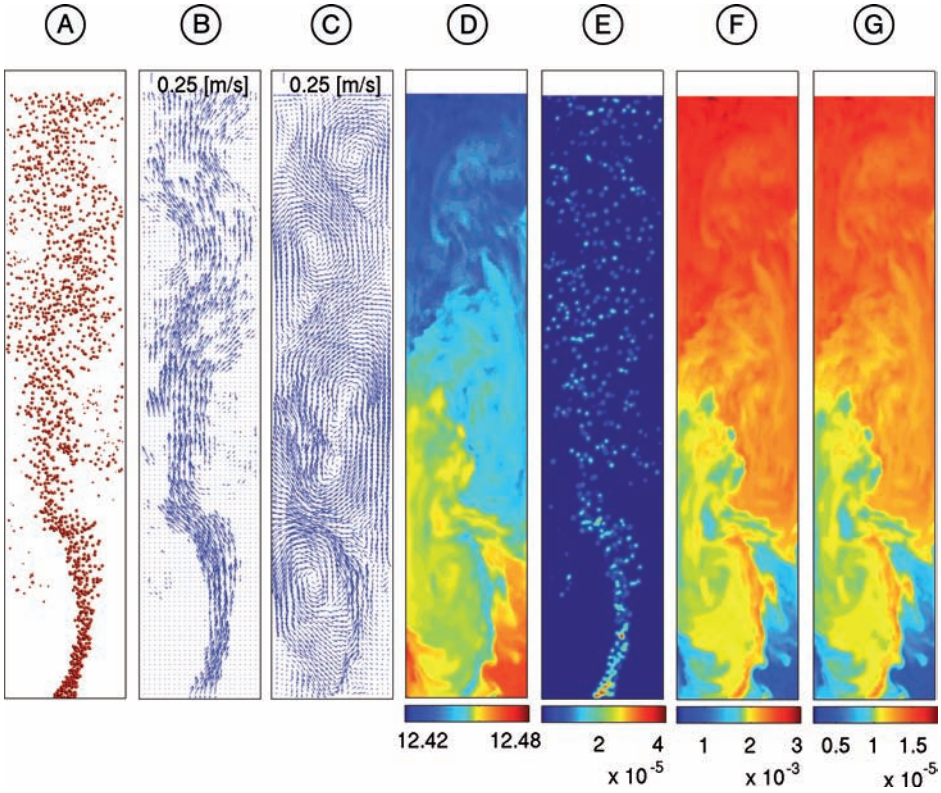

Figure 11. Instantaneous simulation result of a discrete bubble model simulation of chemisorption of CO_2 in an aqueous sodium hydroxide solution with an initial pH = 12.5, 10 s after the CO_2 gas is introduced
A) Bubble positions; B) Gas velocity; C) Liquid velocity; D) pH; E) Concentration of dissolved CO_2, kmol/m^3; F) Concentration of dissolved HCO_3^-, kmol/m^3; G) Concentration of dissolved CO_3^{2-}, kmol/m^3

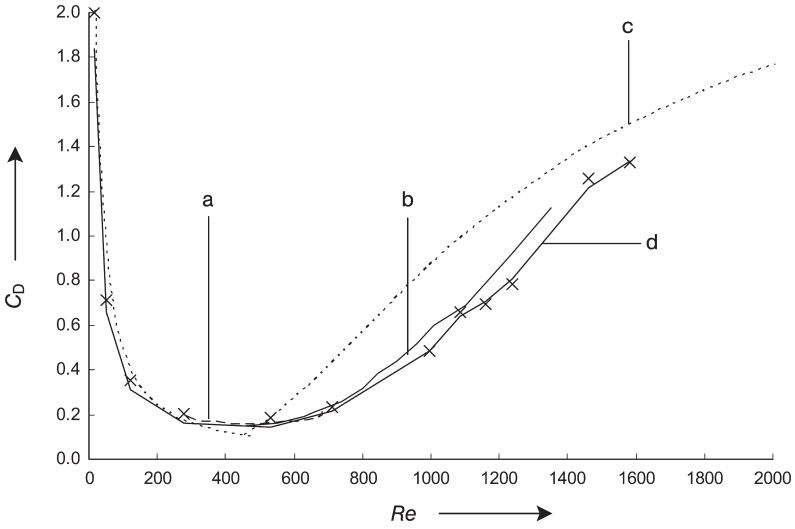

Figure 12. Drag coefficient, C_D, versus Reynolds number, Re, for air bubbles rising in ultrapurified water calculated from DNS (front tracking) simulations [61]
Experimental results (a) by Duineveld [62] and (b) by Veldhuis [63] for ultrapurified water, under conditions comparable to the DNS simulation; experimental results (c) by Tomiyama [64] for clean water, containing only small amounts of contamination; the correlation (d) by Dijkhuizen is fitted through the DNS simulation points
(×) DNS simulation

obtained by TOMIYAMA [60], is recommended:

$$C_L = \begin{cases} \min(0.288\tanh(0.121Re), f(Eo_H)) & Eo_H < 4 \\ f(Eo_H) & 4 \le Eo_H < 10.7 \end{cases}$$

$$f(Eo_H) = 0.00105Eo_H^3 - 0.0159Eo_H^2 - 0.0204Eo_H + 0.474$$

$$Eo_H = \frac{(\rho_L - \rho_G)gd_H^2}{\sigma}$$

This relation involves a modified Eötvös number, Eo, based on the maximum horizontal bubble diameter.

In the homogeneous regime the distance between bubbles is sufficient to assume that a description based on force coefficients of isolated bubbles can be used. For systems with many bubbles, such as in the heterogeneous regime, bubbles generally experience hindered rise, which leads to an increase in the drag force. Relatively little experimental data is available for these systems, since simultaneous measurements of the relevant parameters is very difficult. Instead direct numerical simulations (DNS, see Fig. 9D) can be used to obtain information on the interfacial forces. In DNS, a computational grid size is used which is an order of magnitude smaller than the bubble size. DNS models resolve *all* details of the flow, including bubble shape deformation and oscillation. Contrary to DBM and TFM models no interfacial force closures are required. Instead, DNS can be used to *generate* these force closures that are applied in DBM and TFM models. An example of a thus obtained drag curve for air bubbles in ultra-pure water is shown in Figure 12. The front tracking (FT) technique can easily be extended to study systems with multiple bubbles, to study interfacial forces in bubble swarms (see Fig. 13).

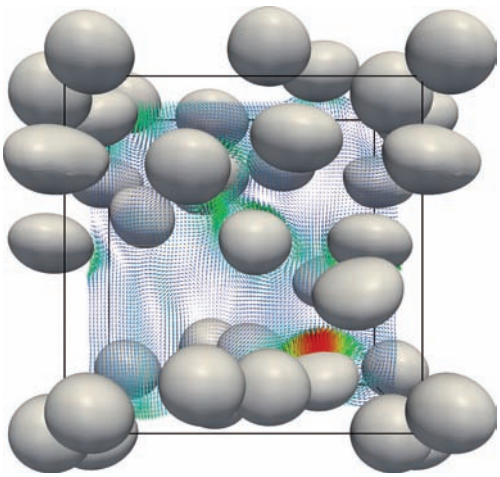

Figure 13. Snapshot of a front tracking simulation of 16 air bubbles with a diameter of 2 mm in water in a cubic domain at a gas fraction of 12% [65]

3. Airlift Loop Reactors

3.1. Design and Applications

Airlift loop reactors are bubbly reactors in which the liquid is brought into a well-organized global circulation via the action of gravity. There are several designs which can be grouped into two different types: internal and external circulation. The former refers to a *single bubble column* in which a riser section and downcomer section are created via an internal shaft. The downcomer is connected to a bubble column, as shown in Figure 14B. Airlift loops (or gas lift loops) can similar to bubble columns process large amounts of gas but have the advantage of a more homogeneous flow and a well defined liquid circulation. This can shorten the mixing times, creating an environment with rather small concentration differences. This can be of advantage, e.g., in bio-applications. Various gas spargers can be found: ring spargers, tube spargers (single or multiple), perforated plates, jets, etc. They may even be equipped with mechanical agitators [66].

Applications in biotechnology are, e.g., fermentation, waste water treatment, ozonation of drinking water, or large scale production of algae in a photo airlift loop [67]. In chemical applications, they are used for e.g., catalytic oxidation of alcohols, direct chlorination of ethylene, or reaction-regeneration of catalysts in the same reactor. In the latter case the well defined circulation inside the airlift is exploited — the desired reaction takes place in e.g., the riser, while the catalyst is regenerated in the downcomer and enters revitalized into the reaction zone.

Gaslifting is also used in the production of oil. In order to reduce the gravitational pressure head on deep wells, gas is injected into the riser connecting the reservoir to the platform.

3.2. Mixing Behavior and Fluid Dynamics

Due to the well-defined liquid circulation in the airlift, the hydrodynamical description of the airlift loop is simpler than of the bubble column. For a first-order model, a one-dimensional approach is sufficient. Here, the flow domain is split in a number of fractions: upward flow in the riser, downward flow (with or without gas bubbles) in the downcomer, separation zone at the top of the airlift, and connection between downcomer and riser. Depending on the design and operation, the downcomer can be single-phase, i.e., 'bubble free', or two-phase, i.e., with bubbles [68], see Figure 15. The latter may be due to recirculation of bubbles into the downcomer when the separation at the top is incomplete or due to additional gas sparging in the downcomer to increase the residence time of the gas phase and the reactor volume in which mass transfer occurs.

Bubble columns and airlift loops are both used as gas–liquid contactors. According to Chisti [69], the operation window for airlift loops is much larger, see Figure 16. However, at present also bubble columns (or slurry columns) operate at higher gas flow rates. For

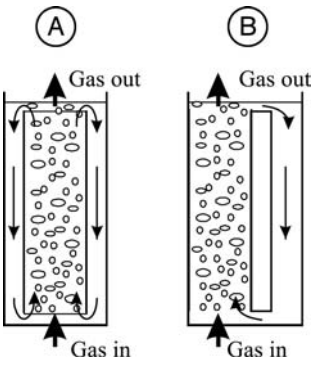

Figure 14. Internal (A) and external (B) airlift loop reactor

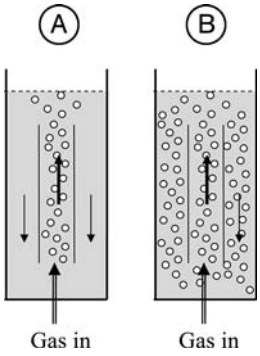

Figure 15. Different flow regimes
A) Complete separation; B) Recirculation of gas

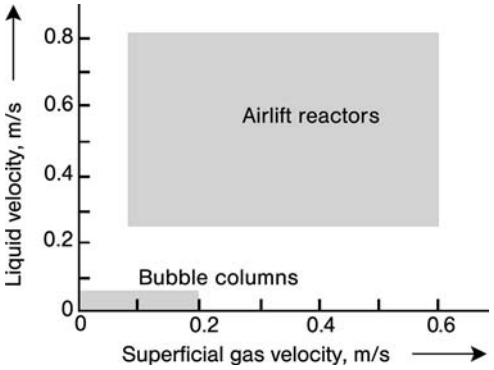

Figure 16. Operation regime of bubble column and airlift reactor [69]

instance, Fischer–Tropsch synthesis slurry reactors operated by Sasol have superficial gas velocities of about 40 cm/s.

In all cases, the driving force for flow is the difference in gas fraction between the riser and downcomer. The friction at the walls and changes in the flow direction are responsible for the dissipation of energy. By balancing the driving force to the friction, a relation between the driving gas fraction difference and the resulting liquid circulation velocity can be found [68, 70–74]:

$$(\varepsilon_{G,R}-\varepsilon_{G,D})(\rho_L-\rho_G)gh_R = K\frac{1}{2}\rho_L v_L^2$$

with ε_G the gas holdup. Note that the velocity in the downcomer is by geometric considerations coupled to the liquid velocity in the riser. Subscripts G, L denote gas and liquid, subscripts R and D indicate riser and downcomer. A second relation between the gas fractions and the liquid velocity is given by the slip velocity for which various models exist.

For one-dimensional flow in steady state, the drift flux model couples the gas fraction to the slip velocity:

$$(1-\varepsilon_G)\frac{j_G}{v_\infty}-\varepsilon_G\frac{j_L}{v_\infty} = \varepsilon_G(1-\varepsilon_G)\frac{v_s}{v_\infty}$$

with j_G, j_L the superficial gas and liquid velocities and v_s the slip velocity of a bubble with respect to the liquid at gas fraction, α_g and the terminal rise velocity of a single, isolated bubble, v_∞. In case of gas recirculation in the downcomer, this relation also couples the downcomer gas fraction to the flow rates in the downcomer.

The slip velocity can be closed via various relations:

- Richardson and Zaki [75]: $\frac{v_s}{v_\infty} = (1-\varepsilon_G)^{n-1}$ The applicable Reynolds and Zaki exponent depending on the Reynolds number is as follows:

Re_∞	n
$Re_\infty < 0.2$	4.65
$0.2 < Re_\infty < 1$	$4.35\ Re_\infty^{-0.03}$
$1 < Re_\infty < 500$	$4.45\ Re_\infty^{-0.1}$
$Re_\infty < 500$	2.39

- Zuber and Findlay [76]: $\varepsilon_G = \frac{j_G}{C_0(j_G+j_L)+\tilde{v}_s}$ The parameters for different flow regimes to be used in the correlation for the gas holdup as suggested by Zuber and Findlay are:

Flow regime	C_0 (–)	$\tilde{v}_s$ (–)
homogeneous	1	0
bubbly	1	$v_\infty(1-\varepsilon_G)^k$ with $k = 1.5 - 3$
churn-turbulent	1.2–1.6	$1.53\left(\frac{\sigma g\Delta\rho}{\rho_L^2}\right)^{1/4}$
slug	1.2–1.45	$0.35\left(g d_t \frac{\Delta\rho}{\rho_L}\right)^{1/2}$

The friction factors are taken from standard correlations, usually from single phase flow. Alternatively, for wall friction a constant Fanning friction $f \approx 0.005$ is taken.

Figure 17 shows the comparison between experiments and modeling for a pilot scale airlift reactor. This graph shows that the model can adequately describe the circulation velocity.

The modeling of an airlift with an internal or external downcomer is similar. The major

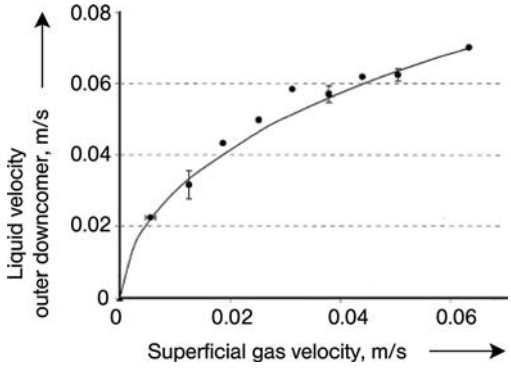

Figure 17. Liquid circulation velocity of a pilot scale airlift (•) Experimental data; (full line) Model prediction (from [68])

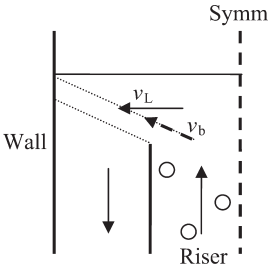

Figure 18. Modeling of gas recirculation into the downcomer

differences are found in the friction factors and the modeling of the gas disengagement zone. The latter can be coarsely approached by a section in which the liquid flows horizontal with a uniform velocity profile, as sketched in Figure 18. The bubbles have a constant vertical slip velocity with respect to the liquid phase and zero slip in the horizontal direction. This way, the separation line can be found for those bubbles that, coming out of the riser, just manage to escape in the disengagement section. All bubbles with trajectories below this separation line flow into the downcomer. In a one-dimensional approach this is dictated only by the gas slip velocity, the circulation velocity and the geometry of the airlift.

3.3. Gas Holdup

The gas holdup in an airlift reactor can be found from the hydrodynamic modeling presented in the previous section. Generally, the gas holdup in an airlift is lower than in a bubble column at the same superficial gas velocity due to the upward liquid flow in the riser. However, the difference is relatively small because at higher superficial gas velocities, bubble columns develop an internal circulation as well.

The gas holdup is influenced by the slip velocity of the bubbles, which is a function of the bubble size. The latter is a function of the gas fraction, the liquid and gas properties (coalescing or noncoalescing medium), and purity of the system as well as of the flow. According to HINZE [77] the maximum stable bubble size in a turbulent flow is given by:

$$d_{b,max} = k\left(\frac{\sigma}{\rho_L}\right)^{0.6} e_V^{-0.4}$$

with e_V being the dissipation of turbulent kinetic energy in the system. HINZE estimated the coefficient k to be 0.725. The energy dissipation can be estimated from the total wall friction from the energy put into the system via the gas inflow. The latter follows as

$$\dot{E}_{in} = \Phi_G \Delta p \approx A_{riser} u (1-\varepsilon_{G,riser}) \rho_L g h_{riser}$$

and consequently

$$e_V \equiv \frac{\dot{E}_{in}}{m} \approx \frac{A_{riser}}{A_{tot}} (1-\varepsilon_{G,riser}) g u$$

with A_{riser} and A_{tot} the cross-sectional area of the riser and total reactor, respectively, u the superficial gas velocity based on the riser cross-section, h_{riser} the riser height, Φ_G the gas inflow rate and Δp the pressure drop from inlet to outlet.

3.4. Mass Transfer and Mixing

The mass transfer is usually specified by the product of the mass transfer coefficient at the liquid side, k_L, and the gas–liquid interface per unit volume, a. For airlift loops, $k_L a$ values are reported in the range of 10^{-3}–10^{-1} s^{-1}. The interfacial area is estimated from

$$a = \frac{6\varepsilon_G}{d_{bS}}$$

The mass transfer coefficient k_L is more difficult to find. An estimate can be obtained from HIGBIE's penetration theory [78]:

$$k_L = 2\sqrt{\frac{D_L v_s}{\pi d_b}} \tag{28}$$

with D_L the diffusion coefficient in the liquid phase, v_s the bubble slip velocity and d_b the bubble diameter. However, this describes the mass transfer only for dilute systems, i.e., at low gas fractions.

MERCHUK et al. [79] studied mixing and mass transfer in concentric tube airlift reactors and found their data on mass transfer to correlate as:

$$Sh = 3\cdot 10^4 Fr^{0.97} M^{-5.4} Ga^{0.045} \left(1-\frac{A_d}{A_{riser}}\right)^{-1}$$

The Sherwood number and the Froude number are defined as $Sh = \frac{k_L a d_t^2}{D_L}$ and $Fr = \frac{u_G}{\sqrt{g d_t}}$, respectively. M takes the effects of the separator at the top of the airlift into account ($M = \frac{d_s}{4d_t}$, where d_s is the diameter of the sepa-

rator) and the Galileo number is given by $Ga = \frac{g\rho_L^2 d_s^3}{\mu_L^2}$. A_d and A_{riser} are the cross sectional areas of the downcomer and riser, respectively. Jurascik et al. [80] provide the empirical relation $k_L a = K\varepsilon_G^p$ with $K = 0.61\ s^{-1}$ and $p = 1.2$. Their formula is clearly not non-dimensional and can most likely not be widely applied. Couvert et al. [81] used a similar semi-empirical expression and reported a power of 0.84. They mentioned that in the literature values for the power ranging from 0.83 to 1.5 have been reported.

Mixing in airlift loops can be quantified using the Bodenstein number $Bo = \frac{v_L h_R}{D_L}$. According to Chisti [71], an airlift reactor can be considered as perfectly mixed if $Bo < 0.1$ and in plug flow if $Bo > 20$. Sanchez Miron et al. [82] found good agreement between their mixing experiments in air–water and air–sea water airlifts using the relation: $Bo = \beta(Fr^{1/3})^{\lambda}$, with $Fr = \frac{u_G^2}{gd_b}$.

Both β (∼3–5) and λ (∼1.0–1.2) are dimensionless parameters that depend on the reactor design. Sanchez Miron et al. [82] further remark, that virtually all correlations proposed only work well for the reactors on which they were based.

Mudde and Saito [83] studied a bubble column and an upward bubbly pipe flow and found that for the same gas fraction the two are similar: the radial gas fraction profiles were the same, and the radial liquid and bubble velocity profiles of the airlift were offset by the mean superficial liquid velocity comparable to those of the bubble column. This suggests that relations for axial dispersion found in bubble columns could be used in airlifts if nothing else is available.

Vial et al. [84] studied the axial dispersion in two different lab-scale airlift reactors. They found that for the homogeneous, transition, and heterogeneous regime the axial mixing was a consequence of the bubble-induced turbulence and that the single phase contribution could be ignored. The axial dispersion coefficient is for practical purposes equal to the turbulent dispersion coefficient, which the authors modeled as:

$$D_G = 3.1 d_{riser} \max\left(\frac{2l_m}{d_{riser}}\left[\frac{du_L}{d(r/R)}\right]_{0\le r/R\le 1}\right)$$

with $l_m = 2\langle d_b\rangle \frac{\varepsilon_R}{\langle\varepsilon_R\rangle}$ being the mixing length. The coefficient depends on the radial profile of the axial liquid velocity. In these equations, R is the radius of the riser. Furthermore, the mixing length depends on the radial gas fraction profile in the riser, $\varepsilon_R(r)$ (r is the radial coordinate), as well as on the average bubble size. The gas fraction distribution is modeled as a power law:

$$\varepsilon_R = \langle\varepsilon_R\rangle \frac{n+2}{n}\left[1-\left(\frac{r}{R}\right)^n\right]$$

The parameter n varies from 8 in the homogeneous regime to 4 in the churn turbulent regime. For the liquid velocity profile a similar expression is used:

$$u_L = \langle u_L\rangle \frac{m+2}{m}\left[1-\left(\frac{r}{R}\right)^m\right]$$

where m varies from about 2 in the homogeneous to 4 in the churn-turbulent regime. These profiles with the same values are also used to model bubble columns. Note that this gives at best the time averaged distribution of the gas fraction and axial liquid velocity profiles.

If coalescence and breakup occurs there is a broad bubble distribution. This will be encountered in cases of high superficial gas velocities, high circulation rate of the gas through the downcomer into the riser, or low liquid circulation. In that case all quantities are usually based on averaged values (if available) of the bubble size. Krishna and co-workers have proposed a two-class bubble model, large versus small bubbles [85].

Note that the mass transfer is dictated by the product of k_L and a. Smaller bubbles at the same gas fraction lead to a higher value of a and thus contribute to a higher mass transfer. However, smaller bubbles have a lower slip velocity. This has a negative effect on the 'surface renewal' of the bubbles and thus decreases k_L. Moreover, smaller bubbles keep the flow longer in the homogeneous flow regime and therefore reduce the amount of local mixing.

3.5. Heat Transfer

Claims have been made that the heat transfer of airlift loops is a factor of two higher than that of bubble columns. This is attributed to the larger liquid circulation velocity (see e.g., [86]). However, Zaidi et al. [87] reported only an 11%

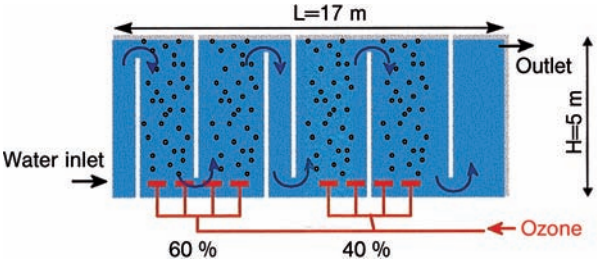

Figure 19. Ozonation tower investigated by Cockx et al. (taken from [96])

increase of the heat transfer coefficient in their experiments of airlift fermenters compared to bubble column fermenters. They propose the following relation for the heat transfer coefficient for air–water bubble columns and internal airlift loops:

$$St = 0.38(ReFr^2)^{-0.32}\left(1+\frac{A_d}{A_{riser}}\right)^{0.05}$$

with $St = \frac{\alpha}{\rho C_p u_G}$, $Re = \frac{u_G d_{riser}\rho_L}{\mu_L}$, and $Fr = \frac{u_G^2}{g d_{riser}}$. d_{riser} refers to the external diameter of the loop; A_d and A_{riser} are the cross sectional area of the downcomer and riser, respectively. Note that for the bubble column $A_d = 0$. The correlation describes the measured data within 4%. The authors provide as margins: $1.4 < ReFr^2 < 8156$ and $0 \leq A_d/A_{riser} < 4.41$. The article also provides a correlation for non-Newtonian liquids.

3.6. Computational Fluid Dynamics

Since the last decade, computational fluid dynamics (CFD) has started to play an increasingly important role in design, modeling and understanding airlift loops. Most simulations are based on the Euler–Euler approach [88–94]. The potential of CFD is obvious: it can give a 3-dimensional, time-dependent, quantitative view of the airlift. Moreover, it can deal with three-phase systems (gas–liquid–solid), [90, 93]. In principle, it can also provide the necessary information on the behavior of the gas knock-out zone, which is difficult to model using analytical tools. Disadvantages are: (1) relatively time consuming, (2) specific CFD-expertise required, (3) uncertainties in modeling closures of the modeling. However, these disadvantages will disappear over time as constant progress is made. A good example can be found in [95], in which oxygen transfer in an airlift reactor is predicted via CFD and compared to experiments. The results indicate that the assumption of a perfectly mixed reactor is questionable. The simulations could capture the deviation from this and show that the oxygen concentration in the bubbles is not constant.

Using CFD, Cockx et al. [89] investigated the ozonation process of drinking water in an industrial ozonation tower (see Fig. 19). The equipment consists of several riser and downcomer sections, separated by weirs. The liquid–bubbly flow is co-current in some parts and counter-current in others. The reactor volume is 350 m^3, i.e., much larger than any lab-scale equipment. The researchers investigated the residence time distribution and made a comparison with experimental data. Subsequently, ozone mass transfer was computed and compared to local measurements for which good agreement was found. Finally, the group reported a successful upgrade of an existing plant using their CFD approach, resulting in a doubling of the disinfection efficiency.

Figure 20 shows one of the CFD results from the article, i.e., the concentration of ozone in the gas phase. Clearly, the concentration is dependent on the location in the tower. A result like this would be very difficult to find from any analytical approach.

Bhole et al. [97] incorporated bubbles of different sizes in the bubbly flow, i.e., they solved a population balance equation for the bubble size. Although, simulations including

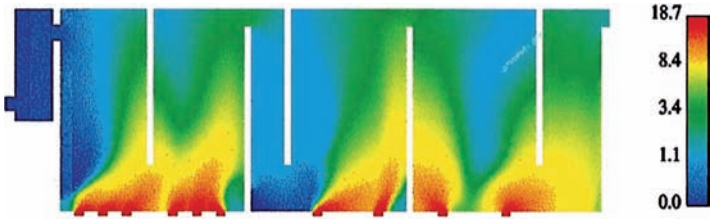

Figure 20. Ozone concentration in the bubble phase (mg/L) (from [95])

variable bubble sizes are by no means mature, they demonstrate a potential and a way forward.

References

1 W.-D. Deckwer, J. Hallensleben, M. Popovic, *Can. J. Chem. Eng.* **58** (1980) 190.
2 H. Buchholz: Reaktionstechnische Untersuchung zur Kultivierung von Hefe in einem Blasensäulenreaktor, Dissertation, Universität Hannover 1979.
3 K. Ruff, T. Pilhofer, A. Mersmann, *Chem.-Ing.-Tech.* **48** (1976) no. 9, 759 – 764.
4 G. Neubauer, T. Pilhofer, *Chem.-Ing.-Tech.* **50** (1978) no. 2, 115 – 116.
5 A. Mersmann, *Ger. Chem. Eng. (Engl. Transl.)* **1** (1978) 1.
6 P. Krötsch, *Fortschr. Verfahrenstech. Abt. D* **16** (1978) 389.
7 P. Zehner, *Chem.-Ing.-Tech.* **47** (1975) no. 5, 209.
8 H. Gerstenberg, *Chem.-Ing.-Tech.* **51** (1979) no. 3, 208 – 216.
9 R.C. Chen, J. Reese, L.-S. Fan, *AIChE J.* **40** (1994) 1093 – 1104.
10 Y.T. Shah, B.G. Kelkar, S.P. Godbole, W.D. Deckwer, *AIChE J.* **28** (1982) 353 – 379.
11 A. Shaikh, M. H. Al–Dahhan, *Int. J. Chem. Reactor Eng.* **5** (2007) R1.
12 A.A. Kulkarni, J.B. Joshi, *Ind. Eng. Chem. Res.* **44** (2005) 5873 – 5931.
13 R. Buchholz, K. Schügerl, *Eur. J. Appl Microbiol. Biotech.* **6** (1979) 301 – 315.
14 E. Blaß, *Chem.-Ing.-Tech.* **60** (1988) no. 12, 935 – 947.
15 P.H. Calderbank, *Chem. Eng.* **45** (1976) CE 209.
16 O. Nagel, B. Hegner, H. Kürten, *Chem.-Ing.-Tech.* **50** (1978) no. 12, 934 – 944.
17 H. Unno, I. Inoue, *Chem. Eng. Sci.* **35** (1980) 1571.
18 K. Akita, F. Yoshida, *Ind. Eng. Chem. Proc. Des. Dev.* **13** (1974) 84 – 91.
19 T. Miyahara, Y. Matsuba, T. Takahashi, *Int. Chem. Eng.* **23** (1983) 517 – 523.
20 T. Miyahara, N. Naga, T. Takahashi, *Int. Chem. Eng.* **23** (1983) 524 – 531.
21 K. Koide, S. Morooka, K. Ueyama, A. Matsuura, F. Yamashita, S. Iwamoto, Y. Kato, H. Inoue, M. Shigeta, S. Suzuki, T. Akehata, *Chem. Eng. Jpn.* **12** (1979) 98 – 104.
22 A. Mersmann, *Chem.-Ing.-Tech.* **61** (1989) , no. 2, 97 – 104.
23 X. Luo, D.J. Lee, R. Lau, G.Q. Yang, L.-S. Fan, *AIChE J.* **45** (1999) 665 – 680.
24 R. Clift, J.R. Grace, M.E. Weber: *Bubbles, Drops, and Particles*, Academic Press, London, 1978.
25 H. Wezorke: *Einfluß von Großblasen in Blasenreaktoren*, Dissertation, Universität Dortmund 1986.
26 R. Beinhauer: Dynamische Messung des relativen Gasgehaltes in Blasensäulen mittels Absorption von Röntgenstrahlen, Dissertation, TU Berlin 1971.
27 H.-P. Riquarts, *Chemie Ingenieur Technik* **52** (1980) 777 – 862.
28 M.H.I. Baird, R.G. Rice, *Chem. Eng. J.* **9** (1975) 171 – 174.
29 J.M. Van Baten, R. Krishna, *Chem. Eng. Sci.* **56** (2001) 503 – 512.
30 K.H. Mangartz, T. Pilhofer, *Verfahrenstechnik* **1** (1980) 40 – 44.
31 H.F. Bach, T. Pilhofer, *Ger. Chem. Eng. (Engl. Transl.)* **1** (1978) 270. H. Buchholz, R. Buchholz, H. Niebeschütz, K. Schügert, *Eur. J. App. Microbiol. Biotechnol.* **6** (1978) 115.
32 K. Akida, F. Yoshida, *Ind. Eng. Chem. Proc.Des. Dev.* **13** (1974) 84 – 91.
33 H. Kölbel, E. Borchers, H. Langemann, *Chem.-Ing.-Tech.* **33** (1961) no. 10, 668 – 675.
34 W. Hikita, S. Asai, K. Tanigawa, K. Segawa, M. Kitao, *Chem. Eng. J.* **20** (1980) 59 – 67.
35 M.H. Oyevaar, K.R. Westerterp, *Chem. Eng. Process.* **25** (1989) 85 – 98.
36 M.H. Oyevaar, R. Bos, K.R. Westerterp, *Chem. Eng. Sci.* **46** (1991) 1217 – 1231.
37 P.M. Wilkinson, L. v. Dierendonck, *Chem. Eng. Sci.* **45** (1990) 2309 – 2315.
38 R. Nottenkämper, A. Steiff, P.M. Weinspach, *Ger. Chem. Eng.* **6** (1983) 147 – 155.
39 J.H. Hills, *Trans. Inst. Chem. Eng.* **52** (1974) 1 – 9.
40 A. Serizawa, I. Kataoka, I. Michiyoshi, *Int. J. Multiphase Flow* **2** (1975) 235 – 246.
41 W.-D. Deckwer, R. Burchhart, G. Zoll, *Chem. Eng. Sci.* **29** (1974) 2177.
42 Y. Kawase, B. Halard, M. Moo-Young, *Chem. Eng. Sci.* **42** (1987) 1609 – 1617.
43 H. Hikita, S. Asai, K. Tanigawa, K. Segawa, M. Kitao, *Chem. Eng. J.* **22** (1981) 61 – 69.
44 J.S. Cho, N. Wakao, *J. Chem. Eng. Jpn.* **21** (1980) 576 – 581.
45 S.P. Godbole, A. Schumpe, Y.T. Shah, N.L. Carr, *AIChEJ.* **30** (1984) 213 – 220.
46 W.-D. Deckwer, *Bubble column reactors*, John Wiley & Sons, Chichester 1991.
47 K. Akita, *Int. Chem. Eng.* **29** (1989) 127 – 135.
48 C. Hulet, P. Clement, P. Tochon, D. Schweich, N. Dromard, J. Anfray, *Int. J. Chem. Reactor Eng.* **7** (2009) R1.
49 J.B. Joshi, Y.T. Shah, *Chem. Eng. Commun.* **11** (1981) 165 – 199.
50 H.A. Jakobsen, B.H. Sannæs, S. Grevskott, H.F. Svendsen, *Ind. Eng. Chem. Res.* **36** (1997) 4052 – 4074.
51 H.A. Jakobsen, H. Lindborg, C.A. Dorao, *Ind. Eng. Chem. Res.* **44** (2005) 5107 – 5151.

52 D. Zhang, N.G. Deen, J.A.M. Kuipers, *Ind. Eng. Chem. Res.* **48** (2009) 47 – 57.
53 S. Lo: "Application of population balance to CFD modelling of bubbly flow via the MUSIG model", *AEA Technology*, AEAT-1096 (1996).
54 E. Olmos, C. Gentric, C. Vial, G. Wild, N. Midoux, *Chem. Eng. Sci.* **56** (2001) 6359 – 6365.
55 D.L. Marchisio, R.D. Vigil, R.O. Fox, *J. Colloid Interf. Sci.* **258** (2003), 322 – 334.
56 J. Sanyal, D.L. Marchisio, R.O. Fox, K. Dhanasekharan, *Ind. Eng. Chem. Res.* **44** (2005) , 5063 – 5072.
57 S. Bove, T. Solberg, B.H. Hjertager, *Chem. Eng. Sci.* **60** (2005) 1449 – 1464.
58 D. Darmana, R.L.B. Henket, N.G. Deen, J.A.M. Kuipers, *Chem. Eng. Sci.* **62** (2007) 2556 – 2575.
59 A. Tomiyama, *Third International Conference on Multiphase Flow, ICMF'98*, Lyon, France, June 8–12, 1998.
60 A. Tomiyama, H. Tamai, I. Zun, S. Hosokawa, *Chem. Eng. Sci.* **57** (2002) 1849 – 1858.
61 W. Dijkhuizen, M. van Sint Annaland, J.A.M. Kuipers, *Chem. Eng. Sci.* (2010) in press.
62 P.C. Duineveld: Bouncing and coalescence of two bubbles in water, Ph.D. thesis, University of Twente, 1994.
63 C. Veldhuis: Leonardo's Paradox: Path and Shape Instabilities of Particles and Bubbles, Ph.D. thesis, University of Twente, 2007.
64 A. Tomiyama, I. Kataoka, I. Zun, T Sakaguchi, *JSME Int. J. Ser. B* **41** (1998) 472 – 479.
65 I. Roghair, M. van Sint Annaland, J.A.M. Kuipers: *Seventh International Conference on CFD in the Minerals and Process Industries CSIRO*, Melbourne, Australia, December 9–11, 2009.
66 Y. Chisti, U.J. Jauregui-Haza, *Biochem. Eng. J.* **10** (2002) 143 – 153.
67 M.J. Barbosa, M. Janssen, N. Ham, J. Tramper, R.H. Wijffels, *Biotechn. Bioeng.* **82** (2003) 170 – 179.
68 W.A.J. Van Benthum, J.H.A. van den Hoogen, R.G.J.M. van der Lans, M.C.M. van Loosdrecht, J.J. Heijnen, *Chem. Eng. Sci.* **54** (1999) 3995 – 4006.
69 M.Y. Chisti, M.M. Young, *Chem. Eng. Comm.* **60** (1987) 195 – 242.
70 J.C. Merchuk, Y. Stein, *AIChE J.* **27** (1981) 377 – 388.
71 M.Y. Chisti: *Airlift bioreactors*, Elsevier Applied Science, London, 1989.
72 W.A.M. Bakker, H.J.L. van Can, J. Tramper, C.D. de Gooijer, *Biotechnol. Bioeng.* **42** (1993) 994.
73 W.A.J. Van Benthum, R.G.J.M. van der Lans, M.C.M. van Loosdrecht, J.J. Heijnen, *Chem. Eng. Sci.* **54** (1999) 3995 – 4006.
74 L. Chraistel, Y. Kawase, H. Znad, *Can. J. Chem. Eng.* **85** (2007) 226 – 232.
75 J.F. Richardson, W.N. Zaki, *Chem. Eng. Sci.* **3** (1954) 65 – 73.
76 N. Zuber, J.A. Findlay, *J. Heat Transfer* **87** (1965) 453 – 468.
77 J.O. Hinze, *AIChE. J.* **1** (1955) 289 – 295.
78 R. Higbie, *Trans. AIChE* **35** (1935) 365 – 389.
79 J.C. Merchuk, N. Ladwa, A. Cameron, M. Bulmer, I. Berzin, A. M. Pickett, *J. Chem. Tech. Biotechnol.* **66** (1996) 174 – 182.
80 M. Jurascik, I. Sikula, M. Rosenberg, J. Markos, *Chem. Biochem. Eng. Quarterly* **21** (2007) 207 – 212.
81 A. Couvert, D. Bastoul, M. Roustan, P. Chetellier, *Can. J. Chem. Eng.* **82** (2004) 914 – 919.
82 A. Sanchez Miron, M.-C. Ceron Garcia, F. Garcia Camacho, E. Molina Grima, Y. Chisti, *Chem. Eng. Res. Des.* **82** (2004) 1367 – 1374.
83 R.F. Mudde, T. Saito, *J. Fluid Mech.* **437** (2001) 203 – 228.
84 C. Vial, S. Poncin, G. Wild, N. Midoux, *Chem. Eng. Sci.* **60** (2005) 5945 – 5954.
85 R. Krishna, J.M. van Baten, M.I. Urseanu, J. Ellenberger, *Catal. Today*, **66** (2001) 199 – 207.
86 P. Weiland, U. Onken, *Ger. Chem. Eng.* **7** (1981) 174.
87 A. Zaidi, S. Alehyen, A. Nassim, *Chem. Eng. Comm.* **155** (1996) 45 – 64.
88 S. Becker, A. Sokolichin, A. G. Eigenberger, *Chem. Eng. Sci.* **49** (1994) 5747.
89 A. Cockx, A. Line, M. Roustan, Z. Do-Quang, V. Lazarova, *Chem. Eng. Sci.* **52** (1997) 3787 – 3793.
90 R.S. Oey, R.F. Mudde, L.M. Portela, H.E.A. van den Akker, *Chem. Eng. Sci.* **56** (2001) 673 – 681.
91 J.M. Van Baten, J. Ellenberger, N. Krishna, *Chem. Eng. Proc.* **42** (2003) 733 – 742.
92 M.S. Vesvikar, M. Al-Dahhan, *Biotech. Bioeng.* **89** (2005) 719 – 732.
93 A. Talvy, A. Cockx, A. Line, *Chem. Eng. Sci.* **60** (2005) 5991 – 6003.
94 A. Talvy, A. Cockx, A. Line, *AIChE J.* **53**, (2007) 335 – 353.
95 A. Talvy, A. Cockx, A. Line, *AIChE J.* **53** (2007) 316 – 326.
96 A. Cockx, Z. Do-Quang, A. Line, M. Roustan, *Chem. Eng. Sci.* **54** (1999) 5085 – 5090.
97 M.R. Bhole, J.B. Joshi, D. Ramkrsihna, *Chem. Eng. Sci.* **63** (2008) 2267.